Electronic states of myricetin

UV-Vis polarization spectroscopy and quantum chemical calculations

Vojta, Danijela; Karlsen, Eva; Spanget-Larsen, Jens

Accepted Manuscript

Electronic states of Myricetin. UV–Vis polarization spectroscopy and quantum chemical calculations

Danijela Vojta, Eva Marie Karlsen, Jens Spanget-Larsen

Please cite this article as: Danijela Vojta, Eva Marie Karlsen, Jens Spanget-Larsen, Electronic states of Myricetin. UV–Vis polarization spectroscopy and quantum chemical calculations, (2016), doi:10.1016/j.saa.2016.09.012

This is a PDF file of an unedited manuscript that has been accepted for publication. As a service to our customers we are providing this early version of the manuscript. The manuscript will undergo copyediting, typesetting, and review of the resulting proof before it is published in its final form. Please note that during the production process errors may be discovered which could affect the content, and all legal disclaimers that apply to the journal pertain.

Electronic states of myricetin. UV-Vis polarization spectroscopy and quantum chemical calculations

Danijela Vojta[a,*], Eva Marie Karlsen[b], Jens Spanget-Larsen[b,*]

[a] Division of Organic Chemistry and Biochemistry, Rudjer Boskovic Institute, Bijenicka 54, 10000 Zagreb, Croatia

[b] Department of Science and Environment, Roskilde University, Postbox 260, Universitetsvej 1, DK-4000 Roskilde, Denmark

This publication is dedicated to Professor Rolf Gleiter on the occasion of his 80th anniversary.

Abstract

Myricetin (3,3',4',5,5',7'-hexahydroxyflavone) was investigated by linear dichroism spectroscopy on molecular samples partially aligned in stretched poly(vinyl alcohol) (PVA). At least five electronic transitions in the range $40000 – 20000$ cm^{-1} were characterized with respect to their wavenumbers, relative intensities, and transition moment directions. The observed bands were assigned to electronic transitions predicted with TD-B3LYP/6-31+G(d,p).

Keywords: Myricetin, UV-Vis polarization spectroscopy, Linear dichroism, Transition moment directions, Time-dependent density functional theory

* Corresponding authors. Tel.:+385 1 457 1220; E-mail: dvojta@irb.hr (D. Vojta), Tel.: 45 4674 2710; E-mail: spanget@ruc.dk (J. Spanget-Larsen)

1. Introduction

Flavonoids are polyphenolic compounds of herbal origin which are brought into animal organisms by consumption of fruits, vegetables, tea or wine. Apart from their nutritive values, they are distinguished by an impressive spectrum of therapeutic actions [1,2] such as antiinflammatory [3] antimicrobial [4] and anticarcinogenic [5,6], as well as by improving cognitive and motorical functions [7]. Myricetin (MCE), a compound that belongs to the flavonol subclass of flavonoids, displays numerous beneficial impacts on humans [8-11] the most highlighted being its high neuroprotective activity [12] manifested through inhibition of the enzyme that metabolizes the drug used in the treatment of Parkinson's disease and, consequently, increasing its bioavailability and efficiency [13].

As for other flavonoids, remarkable antioxidant activity of MCE originates in its capability for free radical scavenging. Even though MCE itself becomes a radical due to this action, the electron delocalization that encompasses planar polycyclic backbone makes the MCE radical one of rather poor reactivity [14]. In addition, six hydroxyl groups enable relatively easy chelation of metal ions which is extremely important when the latter are cell damaging factors.

Successive deprotonation of hydroxyl groups in media of different pH values chemically changes MCE and, consequently, affects its stability and activity [15]. By combining the results obtained from a computational and experimental UV-Vis study, Álvarez-Diduk et al. [16] suggested the most probable mechanism of deprotonation of MCE and demonstrated its decomposition in highly alkaline media (pH $\geq$ 11). Besides the stability being dictated by the pH value of the surrounding medium, Piantanida et al. found that the stability of MCE in ethanol (EtOH) – water mixture is time-dependent and it decomposes after 2-3 hours [17].

The investigations of the activity of MCE generally apply optical spectroscopy as a crucial analytical tool, particularly in the UV-Vis region [15-20]. The electronic transitions of MCE are therefore of considerable interest. Trouillas and coworkers [18] recently performed a theoretical investigation of the UV-Vis spectra for an extensive series of polyphenols, including MCE, focusing on the first strong bands. In order to contribute to the characterization of the electronic transitions of MCE we have investigated the UV-Vis absorption spectrum of the compound in the region $40000 - 20000$ cm^{-1} by means of Linear Dichroism (LD) spectroscopy on molecular samples partially aligned in stretched poly(vinyl alcohol) (PVA), thereby providing information on the polarization directions of the electronic transitions [21,22]. The investigation is supported by the

2

application of quantum chemical computational procedures. Additional information is provided as Supplementary Material (S1 – S10).
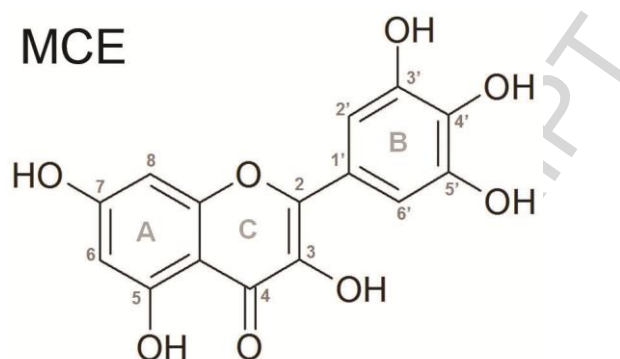
Scheme 1.

2. Calculations

All calculations were performed with the GAUSSIAN09 software package [23]. The equilibrium geometry of MCE was calculated with B3LYP [24,25] density functional theory (DFT) and the 6-31+G(d,p) basis set [22], using an ultrafine grid (int(grid=ultrafine)) [23] and approximating the influence of an alcoholic solvent by the polarized continuum model (PCM) [26] (scrf(pcm,solvent=ethanol)). The most stable conformations of the six hydroxyl groups are found to be those indicated in the molecular diagram in Fig. 1 (detailed structural data and harmonic vibrational wavenumbers are provided as S1). This is consistent with the calculational results of Álvarez-Diduk et al. [16] and with the results of X-ray single crystal and powder diffraction experiments [27]. Starting with a planar geometry (C_s symmetry), a planar molecular structure is predicted with no imaginary frequencies, indicating a true equilibrium structure (S1). However, allowing the molecule to be non-planar leads to the prediction of an equilibrium structure with a slight twist around the 1'–2 bond (linking the pyrogallol and benzopyranone moieties). This is indicated in Fig. 1 which displays the results of a relaxed potential energy scan of the torsional profile, revealing shallow double minima structures close to the torsional angles $\theta = 0°$ and $\theta = 180°$. We have no obvious explanation for the phenomenon; one may speculate that it may be related to different constructions of the integration grid for the (exact) C_s and C_1 symmetries. In the ensuing applications we shall assume that the molecule is effectively planar. Transition to the lowest excited singlet state (2 ^{1}A', see below) increases the tendency towards planarity: In the excited state equilibrium geometry, the 1'–2 bond is shortened from 1.466 to 1.426 Å, and the

corresponding torsional wavenumber is increased from 4.2 to 12.7 cm^{-1}, relative to the ground state. Geometry optimization of the excited state did not lead to tautomerization, corresponding to Excited State Intramolecular Proton Transfer (ESIPT) [20]. We have not pursued this question further as an ESIPT phenomenon would not be observed in the present absorption spectroscopic experiment.

Vertical transitions to excited singlet electronic states of MCE were computed by using the time dependent TD-B3LYP procedure [28] with the 6-31+G(d,p) basis set. The influence of the solvent on the calculated transitions was investigated. Following the strategy outlined in ref. [30], a discreet/continuum model was applied, considering a variety of hydrogen bonded MCE-ethanol clusters and representing the influence of the bulk of the solvent by the PCM model (solvent=ethanol). But the influence of explicit solvent molecules on the calculated transitions was found to be of minor importance. In the following we present results obtained with the PCM continuum model, without explicit solvent molecules. This level of approximation provided excellent results for the electronic transitions of hydroxy-anthraquinone dyes [29-31]. A total of 50 excited states were calculated (S3), but we present only detailed results for transitions in the low-energy region of relevance to this study, see Table 1. In-plane transition moment angles φ are given relative to the first strong transition (2 ^{1}A'), see Fig. 2. Further details are available as supplementary data S2 and S3. A gaussian convolution of the predicted transitions is provided as S4; corresponding results obtained with a selection of TD-DFT procedures are given in S5 – S10.

3. Experimental

3.1. Sample preparation

A sample of MCE was purchased from Extrasynthese ($\geq$ 99 % purity). Polymer sheet material for LD spectroscopy was prepared from PVA powder with average molecular weight 70,000–100,000 Dalton (CAS 9002-98-5, Sigma-Aldrich). Five grams of PVA were dissolved in 50 g distilled water at ca. 90 °C while slowly stirring for several hours. After cooling to room temperature, the homogeneous solution was poured onto a glass plate and left to dry for several days. The resulting polymer sheet was cut into samples of 2×3.5 cm, and the solute was introduced by immersion of the sample pieces for one week in a concentrated solution of MCE in 96% ethanol (Merck Uvasol). The doped samples were dried, cleaned with methanol (Merck Uvasol) to remove crystals from their surface, and uniaxially stretched ca. 600% in the hot stream of air from a hairdryer. To ensure the reproducibility of the results, a number of replicas were produced and investigated. Reference samples were prepared and treated in exactly the same manner, except for the omission of MCE.

Moreover, the stability of MCE in stretched PVA was verified by repeating the measurement after some days; no significant development of the absorption spectrum was observed. Apart from a minor solvent-induced shift, the spectrum observed in PVA compares well with the spectrum observed in EtOH (S4), thereby confirming that MCE is fully protonated in the present experiment [16].

3.2. LD spectroscopy

UV–Vis LD spectra were recorded at room temperature with a Shimadzu UV-2600 spectrophotometer equipped with rotatable Glan prism polarizers as previously described [30-32]. Two linearly independent absorbance curves were measured, one with the electric vector of the sample beam parallel to the stretching direction (U), and one with the electric vector perpendicular to it (V); in both cases the sample beam was perpendicular to the surface of the PVA sheet. The resulting baseline-corrected absorbance curves are denoted by $E_U(\tilde{\nu})$ and $E_V(\tilde{\nu})$; the difference between them, $E_U(\tilde{\nu}) - E_V(\tilde{\nu})$, is defined as the linear dichroism (LD) [21,22]. An example of the recorded curves is shown in Fig. 3.

4. Results and discussion

4.1. Linear dichroism: orientation factors and partial absorbance curves

The directional information that can be extracted from the curves $E_U(\tilde{\nu})$ and $E_V(\tilde{\nu})$ (Fig. 3) is provided by the orientation factors K_i for the molecular transition moments of the observed transitions i [21]:

$$K_i = \left\langle \cos^2(\boldsymbol{M}_i, U) \right\rangle \tag{1}$$

Here ($\boldsymbol{M}_i$, U) is the angle between the transition moment vector $\boldsymbol{M}_i$ of the ith transition and the uniaxial stretching direction U of the polymer sample. The pointed brackets indicate averaging over all molecules in the light path. A large orientation factor K_i thus indicates efficient alignment of the molecular transition moment vector $\boldsymbol{M}_i$ with the sample axis U, and vice versa. The K_i values were determined by the graphical "trial-and-error" (TEM) procedure [21] which involves formation of linear combinations of $E_U(\tilde{\nu})$ and $E_V(\tilde{\nu})$, for example the reduced absorbance curves $r_K(\tilde{\nu})$ [32]:

$$r_K(\tilde{\nu}) = (1-K)E_U(\tilde{\nu}) - 2KE_V(\tilde{\nu}). \tag{2}$$

5

A spectral feature due to transition i (a peak or a shoulder) will vanish from the linear combination $r_K(\tilde{v})$ for $K = K_i$, and the value of K_i can thus be determined by visual inspection [32]. A family of reduced absorbance curves $r_K(\tilde{v})$ for MCE is shown in Fig. 3. A well-defined orientation factor $K = 0.47$ can be determined for the first strong band A with maximum at 25600 cm^{-1}. For the following spectral features B, C, D, and E, the orientation factors can only be determined with reduced accuracy because of broad, overlapping bands. K values close to 0.5 can be estimated for B and E at 30000 and 38800 cm^{-1}, and values close to 0.3 for C and D at 33100 and 36800 cm^{-1}.

The analysis of the observed LD data is further complicated by the low molecular symmetry of MCE; the C_s molecular symmetry allows infinite possible moment directions for in-plane polarized transitions. For transitions polarized in the molecular plane, the task consists in determination of the angles φ_i formed by the moments of the observed transitions i with a specific, well-defined axis in the plane. Traditionally [21], this axis is chosen as the "orientation axis", that is the molecular axis x corresponding to the largest value of the average cosine squared, $\langle \cos^2(x,U) \rangle = K_x$, also called the "long axis" of the molecule. This axis can frequently be estimated from the molecular shape; but in the case of a polar and protic compound like MCE aligned in a polar and protic medium like stretched PVA, other factors than the molecular shape may be important [30]. Additional information would be provided by polarization spectroscopy in the IR region, for example observation of the LD of the carbonyl stretching band. Unfortunately, PVA absorbs strongly in the IR region, and in general, this medium does not allow useful LD IR investigations. We shall assume that the orientation axis x approximately coincides with the moment vector of the first strong transition A at 25600 cm^{-1} with K close to 0.5. The calculated moment direction for this transition is essentially parallel to the 1'–2 bond axis; assignment of this axis as the orientation axis x seems plausible (Fig. 2). The in-plane axis y that is perpendicular to x corresponds to the lowest average cosine squared among directions in the plane, $\langle \cos^2(y,U) \rangle = K_y$. For an in-plane polarized transition i the following relation holds [21]:

$$|\varphi_i| = \tan^{-1} \sqrt{\frac{K_x - K_i}{K_i - K_y}} \tag{3}$$

Provided the orientation factors K_x and K_y for the in-plane axes x and y can be derived, the numerical values of the individual transition moment angles φ_i can thus be determined from the observed K_i values. According to our assignment of the orientation axis, $K_x = 0.5$; the value of K_y must be less than K_x, but is likely to be larger than $(1 - K_x)/2 = 0.25$ [21]. Under the assumptions

6

$(K_x, K_y) \approx (0.5, 0.3)$, Equation (3) predicts that the features A, B, and E with K_i close to 0.5 are essentially x-polarized ($\varphi \approx 0°$), and that the features C and D with K_i close to 0.3 are essentially y-polarized ($\varphi \approx \pm 90°$; the moment angles $+90°$ and $-90°$ are equivalent). But in view of the assumptions made and the approximate nature of most of the experimental K values, these predictions must be considered as qualitative; one should be careful not to overestimate the information content of the LD data [33,34].

In a spectral region where only transitions corresponding to two different K values, such as K_x and K_y, contribute to the observed absorption, it is possible to derive the partial absorbance curves $A_x(\tilde{\nu})$ and $A_y(\tilde{\nu})$ [21,32]:

$$A_x(\tilde{\nu}) = (K_x - K_y)^{-1} r_{K_y}(\tilde{\nu})$$

$$A_y(\tilde{\nu}) = (K_y - K_x)^{-1} r_{K_x}(\tilde{\nu}) \qquad (4)$$

Within the assumptions made, it is thus possible to construct the pair of partial absorbance curves $A_x(\tilde{\nu})$ and $A_y(\tilde{\nu})$ shown in Fig. 4, corresponding to contributions with $K_x = 0.47$ and $K_y = 0.3$. $A_x(\tilde{\nu})$ and $A_y(\tilde{\nu})$ indicate absorbance with moment angles φ close to $0°$ and $\pm 90°$, corresponding to predominantly long- and short-axis polarized absorption, respectively. The polarization assignments are reasonably consistent with the calculated transition moment directions (see below).

4.2. Electronic transitions

The observed transitions are listed in Table 1, where they are compared with the predicted transitions. Observed and predicted transitions are furthermore compared in Fig. 4. It must be emphasized that precise characterization of the observed polarization data is complicated by low molecular symmetry and by broad and overlapping bands (see above). The suggested derivation of transition moment directions from the LD absorption curves relies on a number of assumptions (Section 4.1), and the polarization analysis should be considered as qualitative.

The strong, long-axis polarized band A with maximum at 25600 cm^{-1} is the most important feature of the UV-vis spectrum and is responsible for the color of the compound. This band must be assigned to the 2 ^{1}A' state predicted at 26000 cm^{-1} with oscillator strength $f = 0.60$. The transition is well described by promotion of an electron from the HOMO to the LUMO, listed as [1, −1] in Table 1. As indicated by the π orbital amplitudes shown in Fig. 5, the HOMO is anti-bonding and the LUMO is bonding with respect to the 1'–2 linkage. The predicted transition is thus sensitive to the dihedral angle θ (Fig. 1): For a twisted conformation with $\theta = 90°$ the calculated

7

transition is blue-shifted to 29600 cm^{-1} and the intensity is reduced to $f = 0.17$. Moreover, the transition leads to increased tendency towards planarity as discussed in Section 2. Both HOMO and LUMO are delocalized over most of the molecule, so no massive charge transfer is expected to be associated with the transition. The predicted dipole moments are 5.58 D for the 1 ^{1}A' ground state and 6.88 D for the 2 ^{1}A' excited state (equilibrium geometries), indicating a minor increase of the polarity of the molecule on excitation.

As part of an extensive TD-DFT survey of the electronic transitions of natural polyphenols, Trouillas and coworkers [18] computed the first strong transition of MCE using B3P86/6-311+G(d,p). Compared with the present investigation, these authors obtained similar results with respect to wavenumber and oscillator strength, but they described the transition as 64% HOMO–LUMO. This is at variance with the present percentage of 96%. We wonder whether the percentage was correctly derived by Trouillas and coworkers [18].

The feature B around 30000 cm^{-1} appears as a diffuse shoulder on the tail of band A. Characterization of this shoulder is complicated by the overlap with much stronger absorption A. We tentatively assign the feature B to the states 3 ^{1}A' and 4 ^{1}A' predicted at 29600 and 29900 cm^{-1}. The moment angles φ predicted for transitions to the two states are +8° and –28°, which seems fairly consistent with the predominantly long-axis polarization of the shoulder ($\varphi \approx 0°$).

Band C at 33100 cm^{-1} is predominantly short-axis polarized ($\varphi \approx \pm90°$) and can probably be assigned to the 5 ^{1}A' state predicted at 34100 cm^{-1} with $\varphi = -81°$.

The feature D at 36800 cm^{-1} appears as a shoulder in the isotropic spectrum E_{ISO} but as a peak in the partial absorbance curve A_y (Fig. 4). Like band C, band D is predominantly short-axis polarized ($\varphi \approx \pm90°$), and it can be assigned to the 5 ^{1}A' state predicted at 37200 cm^{-1} with $\varphi = +85°$. The weaker 6 ^{1}A' state calculated at 37400 cm^{-1} probably contributes to this band.

Finally, band E appears as a relatively strong, long-axis polarized peak at 38800 cm^{-1}. This band can be assigned to the 9 ^{1}A' state predicted at 39700 cm^{-1} with $\varphi = -18°$.

5. Concluding remarks

This paper reports the results of a polarization spectroscopic study of molecular samples of MCE partially aligned in a stretched polymer matrix. The investigation lead to resolution of otherwise poorly resolved spectral features. It was thus possible to characterize at least five electronic transitions in the 40000 – 20000 cm^{-1} region. In spite of low molecular symmetry and overlapping

band features, it was possible to derive approximate partial absorbance spectra from the observed linear dichroic curves, indicating qualitative polarization directions (transition moment angles) for the observed spectral features. The results of a TD-B3LYP calculation within the assumption of a planar molecular geometry lead to satisfactory agreement with the observed transitions, including wavenumbers, relative intensities, and moment angles.

Acknowledgements

Table 1. Observed and calculated electronic transitions for myricetin (MCE).

	Observed				TD-B3LYP[a]				
	$\tilde{\nu}^{\,b,c}$	$A^{\,c,d}$	$K^{\,e}$	$|\varphi|^{\,f}$	Term	$\tilde{\nu}^{\,b}$	$f^{\,g}$	$\varphi^{\,f}$	Leading configurations [h]
A	25.6	0.30	0.47	~0°	2 ^{1}A'	26.0	0.60	0°	96% [1, −1]
B	(30.0)	(0.13)	0.5	~0°	3 ^{1}A'	29.6	0.03	+8°	96% [2, −1]
					4 ^{1}A'	29.9	0.07	−28°	95% [3, −1]
C	33.1	0.13	0.3	~90°	5 ^{1}A'	34.1	0.06	−81°	73% [4, −1]
					1 ^{1}A"	36.2	<10^{-4}	z	97% [6, −1]
D	(36.8)	(0.24)	0.3	~90°	6 ^{1}A'	37.2	0.16	+85°	39% [1, −2]; 32% [5, −1]
					7 ^{1}A'	37.4	0.03	−61°	59% [5, −1]; 31% [1, −2]
					2 ^{1}A"	38.8	10^{-3}	z	93% [1, −4]
					8 ^{1}A'	39.4	0.01	+88°	25% [2, −2]; 24% [1, −3]
E	38.8	0.29	0.5	~0°	9 ^{1}A'	39.7	0.25	−18°	39% [2, −2]; 24% [3, −2]
					10 ^{1}A'	41.1	0.04	−43°	47% [1, −3]; 32% [3, −2]
					3 ^{1}A"	41.7	<10^{-4}	z	84% [1, −6]
					11 ^{1}A'	42.4	0.09	+43°	47% [1, −5]; 30% [2, −2]

[a] Complete listings provided as supplementary material (S2, S3).

[b] Wavenumbers in 10^3 cm^{-1}.

[c] Entries in parentheses indicate shoulders in the isotropic spectrum E_{ISO} in Fig. 4.

[d] Absorbances corresponding to features in the isotropic spectrum E_{ISO} in Fig. 4.

[e] Orientation factor, see text.

[f] In-plane transition moment angle φ, see Fig. 2 (z designates out-of-plane polarization).

[g] Oscillator strength.

[h] The notation [i, −j] indicates an excited singlet configuration derived by promotion of an electron from the ith highest occupied to the jth lowest unoccupied molecular orbital.
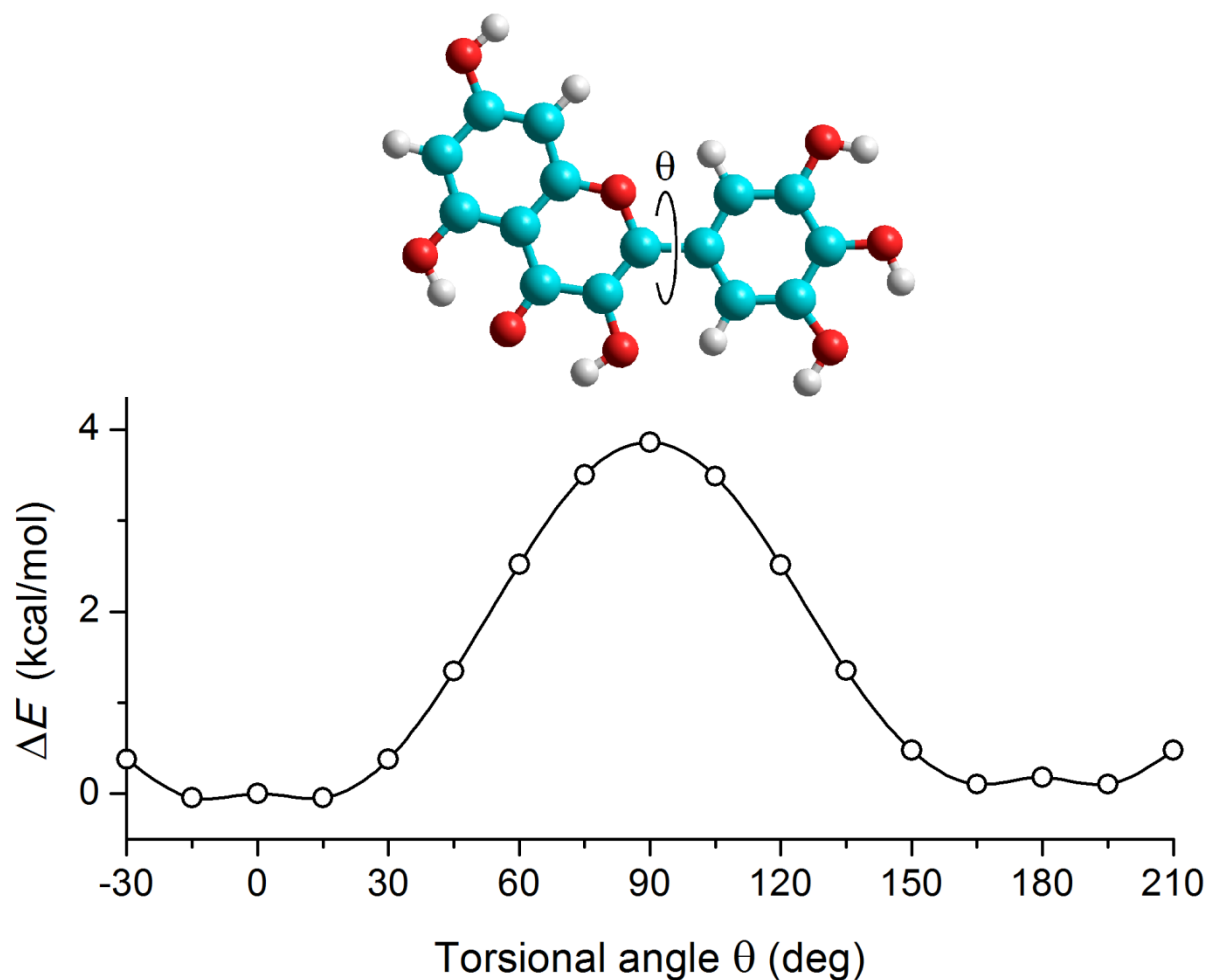
10

Figures

Fig. 1.

Torsional potential energy profile for rotation around the 1'–2 bond of myricetin (MCE) computed with B3LYP/6-31+G(d,p). The torsional angle θ is taken to be zero for the planar conformation indicated.
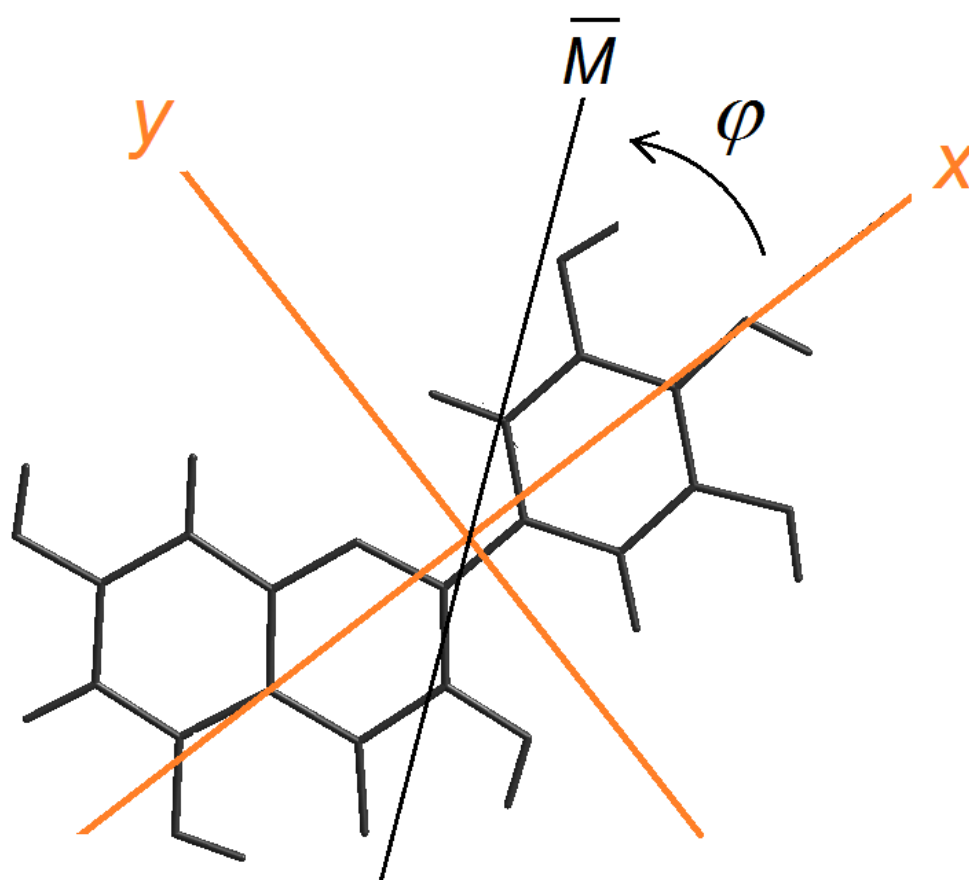
Fig. 2.

Definition of in-plane molecular *x,y* coordinate system for myricetin (MCE). The orientation axis *x* is assumed to coincide with the transition moment vector predicted with TD-B3LYP/6-31+G(d,p) for the first strong transition (2 ^{1}A'). As indicated, in-plane transition moment angles φ are given relative to this axis (see text).
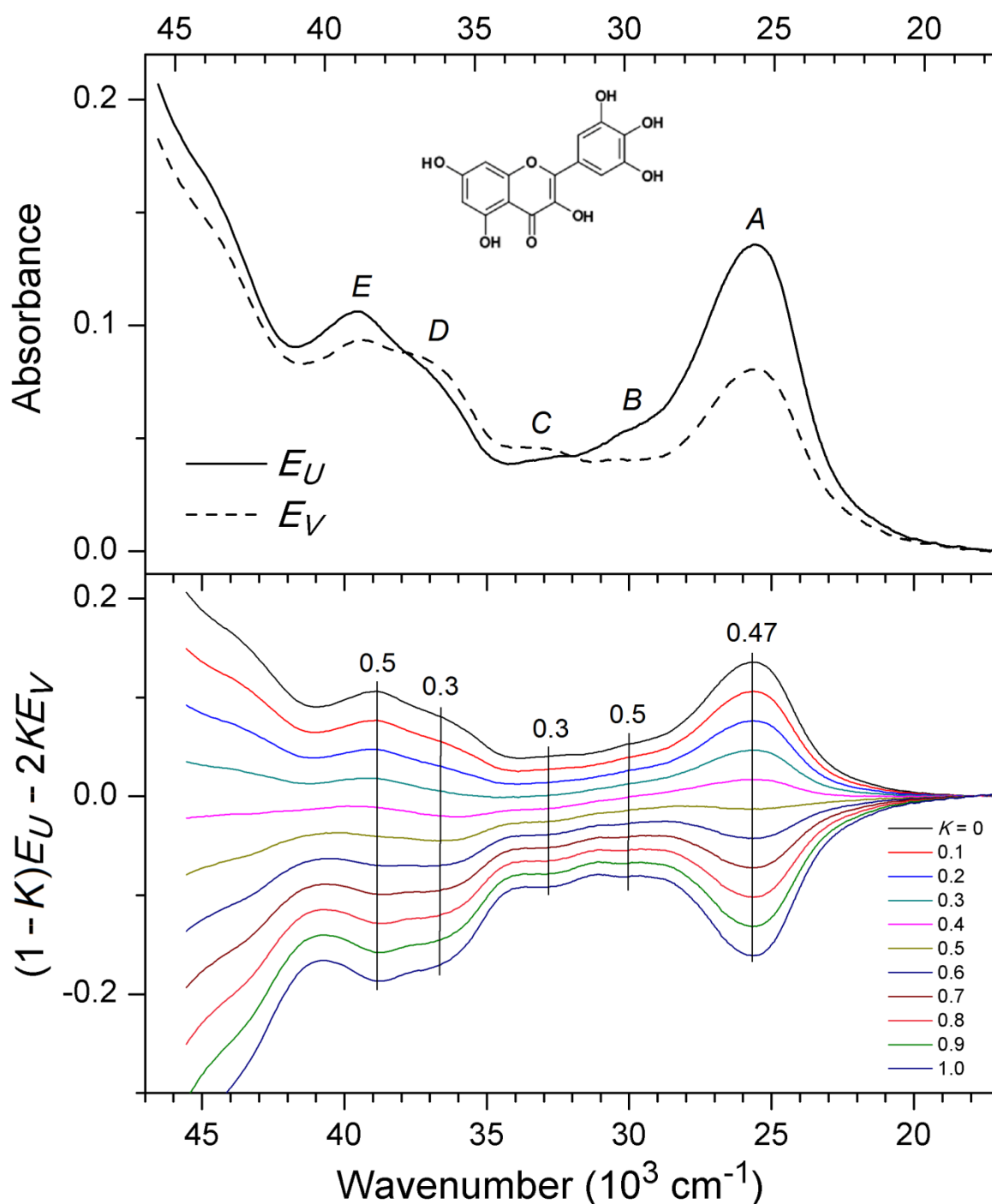
Fig. 3.

(*top*) Observed LD absorbance curves for myricetin (MCE) recorded in stretched PVA. E_U and E_V indicate absorbance measured with the electric vector of the sample beam parallel (*U*) and perpendicular (*V*) to the stretching direction. (*bottom*) Family of reduced absorbance curves according to Equation (2) with *K* values ranging from 0.0 to 1.0 in steps of 0.1. *K* values determined for significant features are indicated.
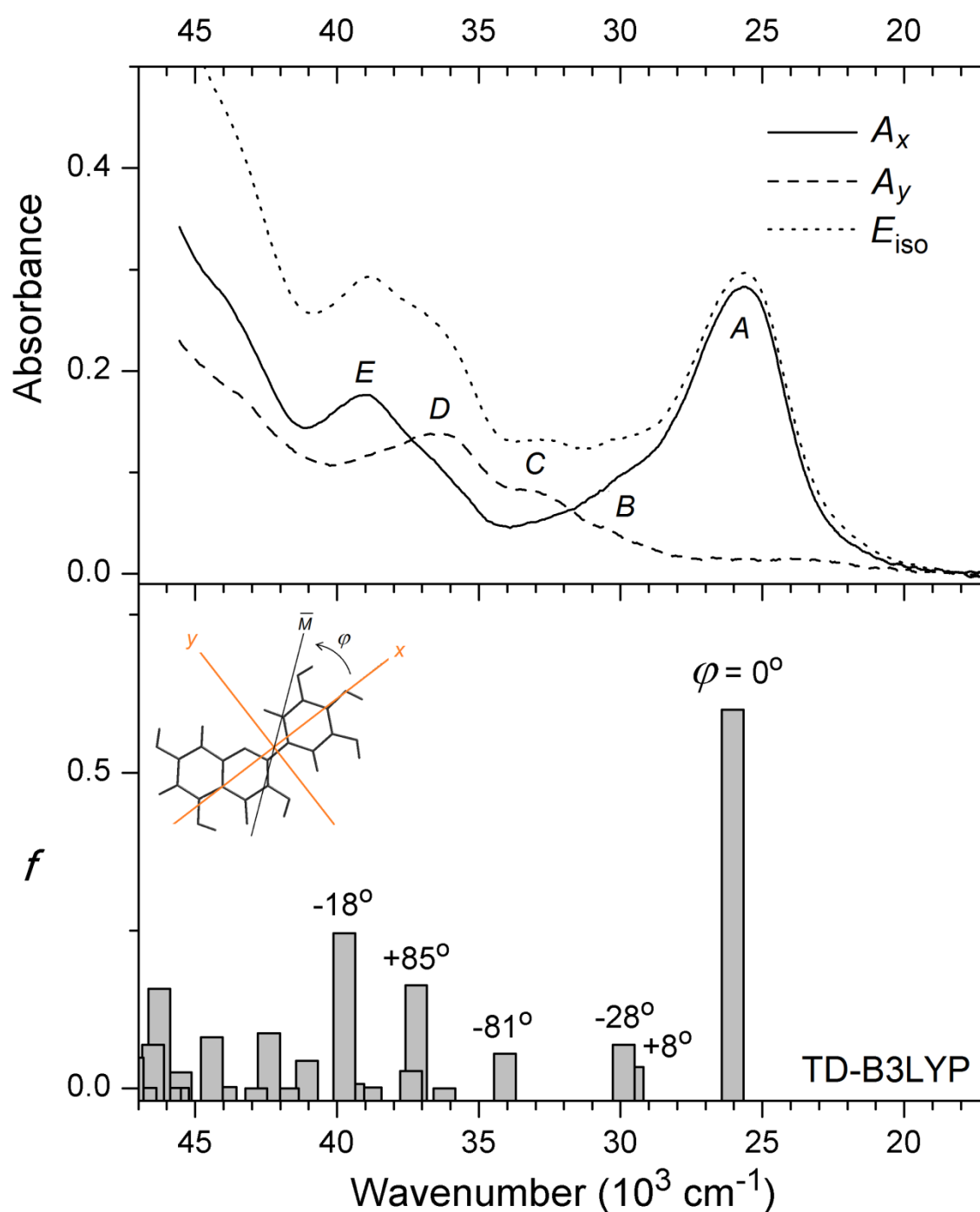
Fig. 4.

(*top*) Tentative partial absorbance curves according to Equations (4) produced with $(K_x, K_y) = (0.47, 0.3)$. A_x and A_y indicate absorbance polarized approximately parallel ($|\varphi| \approx 0°$) and perpendicular ($|\varphi| \approx 90°$), respectively, to the long molecular axis (x), see Fig. 2. E_{ISO} indicate the corresponding isotropic absorbance: $E_{ISO} = A_x + A_y = E_U + 2E_V$. (*bottom*) Graphical representation of transitions computed with TD-B3LYP/6-31+G(d,p), see Table 1.
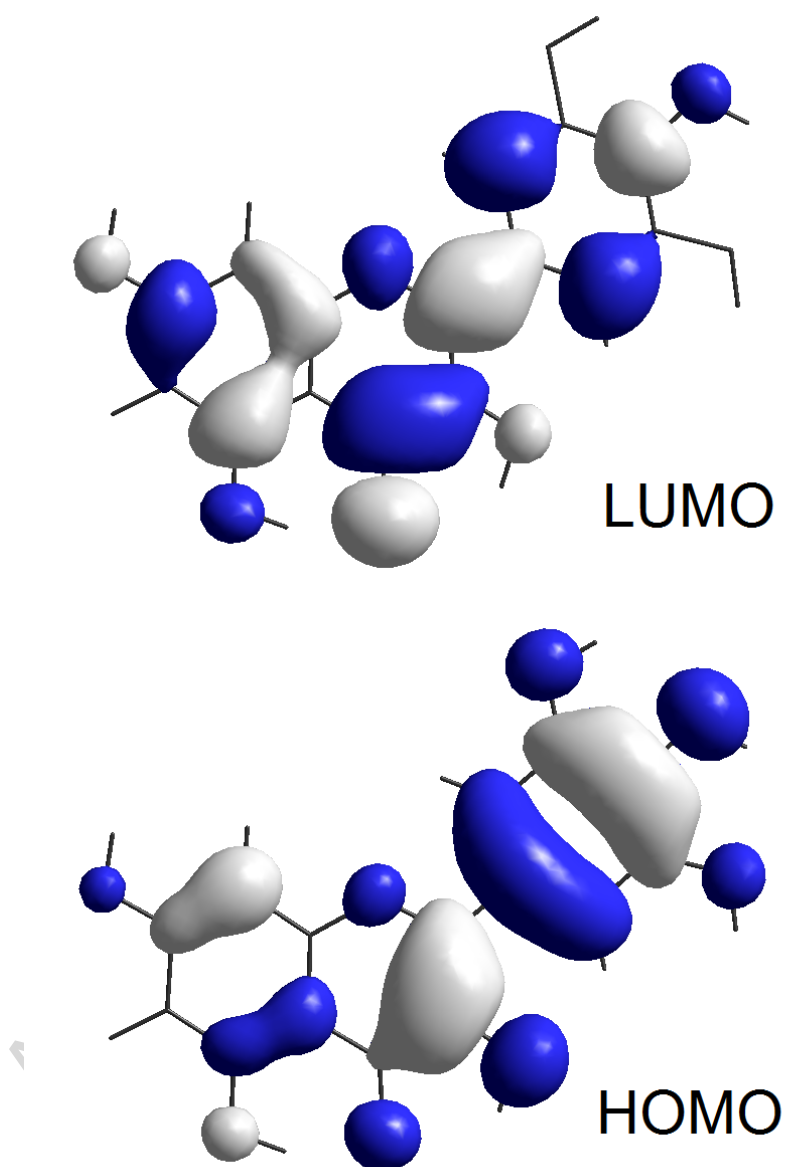
Fig. 5.

Highest occupied molecular orbital HOMO, 15a''(π), and lowest unoccupied molecular orbital LUMO, 16a''(π*), for planar myricetin (MCE).

References:

[1]   A. D. Agrawal, Pharmacological Activities of Flavonoids: A Review, Int. J. Pharm. Sci. Nanotech. 4 (2011) 1394–1398.

[2]   B. Romano, E. Pagano, V. Montanaro, A. L. Fortunato, N. Milić, F. Borrelli, Novel Insights into the Pharmacology of Flavonoids, Phytoter. Res. 27 (2013) 1588–1596.

[3]   Y. S. Tarahovsky, Y. A. Kim, E. A. Yagolnik, E. N. Muzafarov, Flavonoid–membrane interactions: Involvement of flavonoid–metal complexes in raft signaling, Biochim. Biophys. Acta 1838 (2014) 1235–1246.

[4]   J. P. Dzoyem, H. Hamamoto, B. Ngameni, B. T. Ngadjui, K. Sekimizu, Antimicrobial action mechanism of flavonoids from Dorstenia species, Drug Discov. Ther. 7 (2013) 66–72.

[5]   T. Bansal, M. Jaggi, R. K. Khar, S. Talegaonkar, Emerging significance of flavonoids as P-glycoprotein inhibitors in cancer chemotherapy, J. Pharm. Pharmaceut. Sci. 12 (2009) 46–78.

[6]   C. W. How, J. A. Teruel, A. Ortiz, M. F. Montenegro, J. N. Rodríguez-López, F. J. Aranda, Effects of a synthetic antitumoral catechin and its tyrosinase-processed product on the structural properties of phosphatidylcholine membranes, Biochim. Biophys Acta 1838 (2014) 1215–1224.

[7]   M. Jazvinšćak Jembrek, L. Vuković, J. Puhović, J. Erhardt, N. Oršolić, Neuroprotective effect of quercetin against hydrogen peroxide-induced oxidative injury in P19 neurons, J. Mol. Neurosci. 47 (2012) 286–299.

[8]   J. Lu, L. V. Papp, J. Fang, S. Rodriguez-Nieto, B. Zhivotovsky, A. Holmgren, Inhibition of Mammalian Thioredoxin Reductase by Some Flavonoids: Implications for Myricetin and Quercetin Anticancer Activity, Cancer Res. 66 (2006) 4410–4418.

[9]   N. J. Kang, S. K. Jung, K. W. Lee, H. J. Lee, Myricetin is a potent chemopreventive phytochemical in skin carcinogenesis, Ann. N. Y. Acad. Sci. 1229 (2011) 124–132.

[10]   S.-J. Choi, S.-C. Shin, J.-S. Choi, Effects of Myricetin on the Bioavailability of Doxorubicin for Oral Drug Delivery in Rats: Possible Role of CYP3A4 and P-glycoprotein Inhibition by Myricetin, Arch. Pharm. Res. 34 (2011) 309–315.

[11]   D.-H. Choi, C. Li, J.-S. Choi, Effects of myricetin, an antioxidant, on the pharmacokinetics of losartan and its active metabolite, EXP-3174, in rats: possible role of cytochrome P450

3A4, cytochrome P450 2C9 and P-glycoprotein inhibition by myricetin, Journal of Pharm. Pharmacol. 62 (2010) 908–914.

[12]   A. S. DeToma, J.-S. Choi, J. J. Braymer, M. H. Lim, Myricetin: A Naturally Occurring Regulator of Metal-Induced Amyloid-b Aggregation and Neurotoxicity, ChemBioChem 12 (2011) 1198–1201.

[13]   X. Zhu, Y.H. Jia,   Inhibition of catechol-o-methyltransferase (COMT) by myricetin, dihydromyricetin, and myricitrin, Pharmazie 69 (2014) 183–186.

[14]   D. Amić, D. Davidović-Amić, D. Bešlo, N. Trinajstić, Structure-Radical Scavenging Activity Relationships of Flavonoids, Croat. Chem. Acta 76 (2003) 55–61.

[15]   Z. Jurasekova, C. Domingo, J. V. Garcia-Ramos, S. Sanchez-Cortes, Effect of pH on the chemical modification of quercetin and structurally related flavonoids characterized by optical (UV-visible and Raman) spectroscopy, Phys. Chem. Chem. Phys. 16 (2014) 12802–12811.

[16]   R. Álvarez-Diduk, M. T. Ramírez-Silva, A. Galano, A. Merkoci, Deprotonation Mechanism and Acidity Constants in Aqueous Solution of Flavonols: a Combined Experimental and Theoretical Study, J. Phys. Chem. B 117 (2013) 12347–12359.

[17]   I. Piantanida, L. Mašić, G. Rusak, Structure-spectrophotometric selectivity relationship in interactions of quercetin related flavonoids with double stranded and single stranded RNA, J. Mol. Struct. 924–926 (2009) 138–143.

[18]   E.H. Anouar, J. Gierschner, J.-L. Duroux, P. Trouillas, UV/Visible spectra of natural polyphenols: A time-dependent density functional theory study, Food Chem. 131 (2012) 79–89.

[19]   W. M. Tay, G. F. Z. da Silva, L.-J. Ming, Metal Binding of Flavonoids and Their Distinct Inhibition Mechanisms Toward the Oxidation Activity of Cu^{2+}-β-Amyloid: Not Just Serving as Suicide Antioxidants, Inorg. Chem. 52 (2013) 679–690.

[20]   Y. Wang, Y. Hu, T. Wu, X. Zhou, Y. Shao, Triggered Excited-State Intramolecular Proton Transfer Fluorescence for Selective Triplex DNA Recognition, Anal. Chem. 87 (2015) 11620−11624.

[21]   J. Michl, E.W. Thulstrup, Spectroscopy with Polarized Light, VCH-Wiley, Deerfield Beach, FL, 1986, 1995.

[22]   B. Nordén, A. Rodger, T. Dafforn: Linear Dichroism and Circular Dichroism. A Textbook on Polarized-Light Spectroscopy", RCS Publishing 2010.

[23] M. J. Frisch, G. W. Trucks, H. B. Schlegel, G. E. Scuseria, M. A. Robb, J. R. Cheeseman, G. Scalmani, V. Barone, B. Mennucci, G. A. Petersson, H. Nakatsuji, M. Caricato, X. Li, H. P. Hratchian, A. F. Izmaylov, J. Bloino, G. Zheng, J. L. Sonnenberg, M. Hada, M. Ehara, K. Toyota, R. Fukuda, J. Hasegawa, M. Ishida, T. Nakajima, Y. Honda, O. Kitao, H. Nakai, T. Vreven, J. A. Montgomery, Jr., J. E. Peralta, F. Ogliaro, M. Bearpark, J. J. Heyd, E. Brothers, K. N. Kudin, V. N. Staroverov, R. Kobayashi, J. Normand, K. Raghavachari, A. Rendell, J. C. Burant, S. S. Iyengar, J. Tomasi, M. Cossi, N. Rega, J. M. Millam, M. Klene, J. E. Knox, J. B. Cross, V. Bakken, C. Adamo, J. Jaramillo, R. Gomperts, R. E. Stratmann, O. Yazyev, A. J. Austin, R. Cammi, C. Pomelli, J. W. Ochterski, R. L. Martin, K. Morokuma, V. G. Zakrzewski, G. A. Voth, P. Salvador, J. J. Dannenberg, S. Dapprich, A. D. Daniels, Ö. Farkas, J. B. Foresman, J. V. Ortiz, J. Cioslowski, and D. J. Fox, GAUSSIAN 09, Revision D.01, Gaussian, Inc., Wallingford, CT, 2009.

[24] A.D. Becke, Density-functional thermochemistry. III. The role of exact exchange, J. Chem. Phys. 97 (1992) 9173; 98 (1993) 5648–5652.

[25] C. Lee, W. Yang, R.G. Parr, Development of the Colle-Salvetti correlation-energy formula into a functional of the electron density, Phys. Rev. B 37 (1988) 785–789.

[26] J. Tomasi, B. Mennucci, R. Cammi, Quantum mechanical continuum solvation models, Chem. Rev. 105 (2005) 2999–3093.

[27] M. Sowa, K. Ślepokura, E. Matczak-Jon, A 1:1 pharmaceutical cocrystal of myricetin in combination with uncommon piracetam conformer: X-ray single crystal analysis and mechanochemical synthesis, J. Mol. Struct. 1058 (2014) 114–121.

[28] M.A.L. Marques, C.A. Ullrich, F. Nogueira, A. Rubio, K. Burke, E.K.U. Gross (Eds.), Time-Dependent Density Functional Theory, Lecture Notes in Physics, vol. 706, Springer, Berlin, Heidelberg, New York, 2006.

[29] D. Jacquemin, X. Assfeld, J. Preat, E.A. Perpète, Comparison of theoretical approaches for predicting the UV/Vis spectra of anthraquinones, Mol. Phys. 105 (2007) 325–331.

[30] S.C. Nguyen, B.K.V. Hansen, S.V. Hoffmann, J. Spanget-Larsen, Electronic states of emodin and its conjugate base. Synchrotron linear dichroism spectroscopy and quantum chemical calculations, Chem. Phys. 352 (2008) 167–174.

[31] D.D. Nguyen, N.C. Jones, S.V. Hoffmann, J. Spanget-Larsen, Synchrotron radiation linear dichroism (SRLD) investigation of the electronic transitions of quinizarin, chrysazin, and anthrarufin, Spectrochim. Acta A 77 (2010) 279–286.

[32]   F. Madsen, I. Terpager, K. Olskær, J. Spanget-Larsen, Ultraviolet-visible and infrared linear dichroism spectroscopy of 1,8-dihydroxy-9,10-anthraquinone aligned in stretched polyethylene, Chem. Phys. 165 (1992) 351–360.

[33]   E. W. Thulstrup, P. W. Thulstrup, Polarization Spectroscopic Studies of Ordered Samples, Acta Chim. Slov. 52, (2005) 371–383.

[34]   P. W. Thulstrup, E. W. Thulstrup, Information Content in Linear Dichroism Spectra, Polish J. Chem. 82 (2008) 901–920.
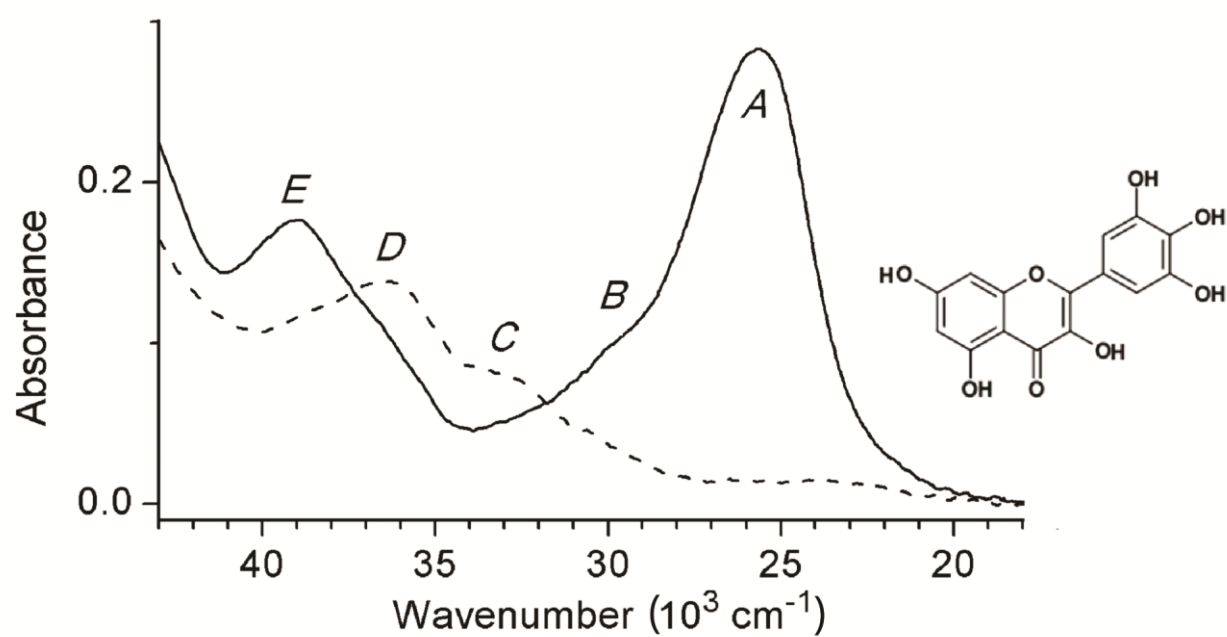
Graphical abstract

Electronic states of myricetin. UV-Vis polarization spectroscopy and quantum chemical calculations

Danijela Vojta[a,*], Eva Marie Karlsen[b], Jens Spanget-Larsen[b,*]

[a] Division of Organic Chemistry and Biochemistry, Rudjer Boskovic Institute, Bijenicka 54, 10000 Zagreb, Croatia

[b] Department of Science and Environment, Roskilde University, Postbox 260, Universitetsvej 1, DK-4000 Roskilde, Denmark

Highlights:

- UV-Vis polarization spectroscopy of myricetin
- Resolution of previously unobserved features
- Five electronic states characterized in the region $40000 - 20000\ cm^{-1}$
- Qualitative transition moment directions derived from the linear dichroic spectra
- Good agreement with transitions predicted by TD-B3LYP calculation